*Journal of Sound and Vibration* (1997) **206**(1), 87–101

# MEASUREMENT OF STRUCTURAL INTENSITY USING A NORMAL MODE APPROACH

L. GAVRIC

*CETIM—Département Acoustique Industrielle*, *BP* 67-60304 *Senlis*, *France*

AND

U. CARLSSON AND L. FENG

*Royal Institute of Technology*, *Technical Acoustics*, *Department of Vehicle Engineering*, *S*-100 44 *Stockholm*, *Sweden*

(*Received* 15 *November* 1996, *and in final form* 25 *April* 1997)

A method is presented for the measurement of structural intensity using a normal mode approach. This method is tested on an assembly of two plates. The structural intensity field and the divergence of structural intensity are evaluated. The power injected into the structure by a shaker is evaluated in two different ways: directly by measuring the force and the velocity at the excitation point, and by integrating the structural intensity vectors over a closed curve containing the vibration source. There is a close agreement between the results obtained by the two methods.



## 1. INTRODUCTION

The concept of structural intensity is introduced in order to extend the vector acoustics approach to energy flow in structure-borne sound fields. This concept is completely analogous to sound intensity, as it represents the same physical quantity, i.e., the net mechanical energy transmitted through a unit surface.

Structural intensity is used to describe the transfer of vibration energy. The spatial distribution of structural intensity within the structure offers information on energy transmission paths and positions of sources and sinks of mechanical energy. Theoretical formulations of structural intensity and corresponding measurement techniques have been developed and successfully applied for various types of simple structural elements (beams, plates, pipes . . .).

The first publications concerning structural intensity appeared in the seventies [1–3]. These papers deal with the theoretical development of the measurement methods. The publications which followed were more concerned with the applications of developed measurement techniques to practical measurements in beams and plates [4, 5]. In reference [6], acoustical holography was used as a tool for the measurement of the structural intensity. References [7–9] deal with the theoretical development of the measurement methods for pipes and shells.

The two types of measurement techniques have been in use so far: one "direct", where fundamental expressions for intensity were suitably adapted for measurement [2, 3, 5], the other based on wave representation of the vibratory field which in turn permitted simplifications [1, 4, 6]. A well designed measurement method represents a compromise between the complexity of the rigorous theoretical formulation and the required simplicity

0022–460X/97/360087 + 15 $25.00/0/sv971077 

of measurement procedures. It has been shown that the measurement accuracy becomes poor with the increase of the complexity of the method applied, which seriously limited the practical use of some measurement techniques.

Of primary practical concern however are assemblies of structural elements. The presence of multiple wave reflections and near fields due to changes in thickness, changes of cross-section, etc., diminishes dramatically the accuracy of most of the measurement methods based on the wave approach and on the far field approximation.

Experimental modal analysis has been widely accepted as the principal investigation tool in the structural dynamics of built-up structures. It therefore seems appropriate to estimate the modal approach in structural intensity measurements in such types of structures. The first attempt to use normal modes in order to evaluate the structural intensity field in built-up structures was performed by Pavic and Gavric [10–13]. In these works the numerical computation of structural intensity by using a finite element technique was considered.

## 2. STRUCTURAL INTENSITY MEASUREMENTS BY MODAL APPROACH—THEORETICAL BACKGROUND

### 2.1. STRUCTURAL INTENSITY

Active structural intensity is a time independent vector quantity defined by the following expression for a given point of structure and for sinusoidal vibration:

$$I_k = -\tfrac{1}{2}\mathscr{R}[\tilde{\sigma}_{kl}\tilde{v}_l^*]. \tag{1}$$

It involves the complex amplitude of the stress tensor $\tilde{\sigma}_{kl}$ and the complex amplitude of the particle velocity vector $\tilde{v}_l^*$. Complex quantities are denoted by a tilde sign, $\mathscr{R}[...]$ represents the real part, while the asterisk denotes complex conjugate. In the case of steady state random vibration the structural intensity is defined by the real part of the cross-spectra between the stress components and corresponding velocity components.

In the following text the proposed technique based on measured modal properties is developed by using the mathematical notation appropriate for sinusoidal vibrations. The corresponding random vibration formulae can easily be deduced from the sinusoidal type ones.

### 2.2. STRUCTURAL INTENSITY AND MODAL PARAMETERS

In any modal approach, the number of modes which enter the analysis has to be appropriately chosen. Usually, for computation of the displacement field or its time derivatives, the number of modes is chosen in such a way that the highest eigenfrequency used in computation is a few times higher than the excitation frequency. This criterion was shown not to be sufficient when structural intensity was concerned [10].

Structural intensity is a result of an interaction between the stresses and the corresponding velocities. The stresses are proportional to the spatial derivatives of the displacements. The spatial distributions of stresses are not as "smooth" as the corresponding distributions of displacements. For example, the bending displacements of a simply supported beam due to a concentrated static force can be represented by a "smooth" polynomial type function, while the corresponding distribution of the lateral shear force has a "jump" at the force position. The same can be observed in the vicinity of any abrupt change of geometry (cross-section, thickness, etc.), or of material properties of the structure. The number of modes sufficient for an accurate estimate of the "smooth" displacement field, generally is not sufficient for the approximation of its spatial derivatives. Therefore the required number of modes for an accurate analysis of dynamic

stresses may increase by one or more orders of magnitude [10–13]. Since the conventional experimental modal analysis cannot deal with such a large number of modes, the higher order modes, necessary for an adequate representation of intensity distribution, have to be accounted for in a more appropriate way. A technique based on approximation of higher order modes by the corresponding quasi-static solution, when computation of structural intensity is concerned, was developed in reference [13]. In the present article a corresponding experimental procedure which relies on measurement of vibrations in operating conditions and on experimental modal analysis is proposed.

The particle velocity of an arbitrary point can be expressed using modal superposition. The particle velocities, defining the vibration of the structure, can be written as a column vector $\{\tilde{\mathbf{v}}_l\}$.

$$\{\tilde{\mathbf{v}}_l\} = -\sum_v \mathrm{j}\omega\tilde{\alpha}_v\{\phi_l\}_v - \mathrm{j}\omega\{\tilde{R}_l\}. \tag{2}$$

Here $\omega$ is frequency, $\{\phi_l\}_v$ is a normal mode shape, $\tilde{\alpha}_v$ is the modal magnification factor, $\mathrm{j} = \sqrt{-1}$ represents the imaginary unit. The modal indexes are denoted by the Greek letters $(\mu, v, \ldots)$. As the number of modes which can be evaluated with a required accuracy is limited, the complex vector $\{\tilde{R}_l\}$ is added in order to compensate for the influence of the higher order modes to the velocity field $\{\tilde{v}_l\}$.

The column vector of dynamics stresses $\{\tilde{\sigma}_{kl}\}$ corresponding to the vibration defined with the velocity field $\{\tilde{v}_l\}$ can also be written by using a modal superposition as

$$\{\tilde{\sigma}_{kl}\} = \sum_v \tilde{\alpha}_v\{\psi_{kl}\}_v + \{\tilde{S}_{kl}\}. \tag{3}$$

Equation (3) involves modal magnification factors $\tilde{\alpha}_\mu$ and column vectors containing stresses $\{\psi_{kl}\}_\mu$ corresponding to the mode shape $\{\phi_l\}_\mu$. A complex stress vector $\{\tilde{S}_{kl}\}$ is added in order to account for the influence of the higher order modes to the stress field.

Note that both the additional stress vector $\{\tilde{S}_{kl}\}$ and modal stresses $\{\psi_{kl}\}_\mu$ are computed by using the displacement-type vector $\{\tilde{R}_l\}$ and mode shape vector $\{\phi_l\}_\mu$. The stress evaluation procedure can be expressed in a form of a linear operator $\Lambda(...)$:

$$\{\psi_{kl}\}_\mu = \Lambda(\{\phi_l\}_\mu), \qquad \{\tilde{S}_{kl}\} = \Lambda(\{\tilde{R}_l\}). \tag{4}$$

The operator $\Lambda(...)$ involves partial derivatives, and geometric and material properties of the structure. For example, the linear operator used to compute the stresses in the axially vibrating bar of cross-section $A$ and modulus of elasticity $E$ takes the form $\Lambda(...) = AE\,\partial(...)/\partial x$. The required partial derivative can be approximated by finite difference techniques.

The structural intensity expressed by modal parameters takes the form

$$\{I_k\} = \mathscr{R}\left[\sum_\mu\sum_v \frac{\mathrm{j}\omega\tilde{\alpha}_\mu\tilde{\alpha}_v^*}{2}\{I_k\}_{\mu v}\right] + \mathscr{R}\left[\sum_v \frac{\mathrm{j}\omega\tilde{\alpha}_v^*}{2}\{\tilde{J}_k\}_v\right] + \ldots, \tag{5}$$

where the vectors $\{I_k\}_{\mu v}$ and $\{\tilde{J}_k\}_v$ are obtained by an appropriate multiplication of the terms of vectors $\{\psi_{kl}\}_\mu$, $\{\phi_l\}_v$ and $\{\tilde{S}_{kl}\}$ according to equation (1):

$$\{I_k\}_{\mu v} = \{\psi_{kl}\phi_l\}_{\mu v}, \qquad \{\tilde{J}_k\}_v = \{\tilde{S}_{kl}\phi_l\}_v. \tag{6}$$

In equations (5) and (6), it is implicitly supposed that the modal superposition gives an accurate approximation of the velocity field. Consequently, the influence of the higher order modes, on the velocity field can be disregarded: $\{\tilde{R}_l\} \approx \{0\}$. This hypothesis is

fulfilled when the number of modes which enter the analysis is approximately selected. Unfortunately, the general rule which defines the number of modes which have to be taken into account in the modal superposition does not exist and an analyst has to rely on experience.

The number of modes which can be extracted by an experimental modal analysis is not sufficient for an accurate representation of dynamic stresses, when structural intensity is concerned. Therefore, the dynamic stresses due to the higher order modes $\{\tilde{S}_{kl}\}$ are not negligible. An abrupt change of stresses, such as occurs in the vicinity of an excitation point, cannot be described by a superposition of a moderate number of lower modal shapes. Usually, such a moderate number of modes is sufficient for the accurate approximation of the velocity field.

To summarize, the structural intensity can be evaluated if the following three quantities are known: the intermodal intensity vectors $\{I_k\}_{\mu\nu}$ computed from the experimentally evaluated mode shapes $\{\phi_l\}_\nu$ and the corresponding modal stresses $\{\psi_{kl}\}_\mu$; the products of the modal magnification factors $\tilde{\alpha}_\mu\tilde{\alpha}_\nu^*/2$; the terms which include the influence of higher order modes $(\tilde{\alpha}_\mu^*/2)\{\tilde{J}_k\}_\mu$.

The mode shapes $\{\phi_l\}_\nu$ can be evaluated by using a conventional experimental modal analysis. The modal stresses $\{\psi_{kl}\}_\mu$ are recalculated by using the experimentally obtained mode shapes $\{\phi_l\}_\mu$ and an appropriate linear operator $\Lambda(...)$, according to equation (4). The linear operator needed for the evaluation of the stress field depends on the type of structure. The method does not impose the same type of operator for the whole structure. Simple structural elements can be treated separately. Different types of operator can be combined and used for the same structure. For example the method permits the treatment of a variety of thin-walled structures by using only two types of linear operator, corresponding to the basic elements of structural assembly: beams and plates.

Both the modal stresses and mode shapes are the function of the structure, only. The other terms involved in equation (5) ($\tilde{\alpha}_\mu\tilde{\alpha}_\nu^*/2$ and $(\tilde{\alpha}_\mu^*/2)\{\tilde{J}_k\}_\mu$) depend on the structural response and must be deduced from additional vibrational measurements in operating conditions.

### 2.3. EVALUATION OF STRUCTURAL INTENSITY USING MEASUREMENTS OF VIBRATION IN OPERATING CONDITIONS

The vibration field of structure is completely defined by the spatial and frequency distributions of particle velocities. In practice the vibrational velocities are evaluated at a finite number of structural points $\{\tilde{v}_k\}$. The usual measurement procedures evaluate the velocity data in a form of quadratic spectral data. The complete set of measurement data then results in a Hermitian type matrix containing the auto-spectral and the cross-spectral data. In general, the vibrational velocity matrix $[\tilde{V}_{kl}]$ is formed by $n(n+1)/2$ measured complex spectra, where $n$ represents the number of measurement points. Note that in the case of a completely correlated vibrational field only $n$ measurements are needed to evaluate vibrational velocity matrix $[\tilde{V}_{kl}]$: auto-power spectrum at reference point $\tilde{v}_R\tilde{v}_R^*/2$ and $n-1$ transfer functions $\tilde{H}_{iR}(\omega) = \tilde{v}_i/\tilde{v}_R$; $R$ and $i$ indicate the reference and the actual measurement point. The vibrational velocity matrix can be expressed by using the modal parameters:

$$[\tilde{V}_{kl}] = \tfrac{1}{2}\{\tilde{v}_k\}\{\tilde{v}_l^*\}^{\mathrm{T}} = \omega^2 \sum_\mu \sum_\nu \frac{\tilde{\alpha}_\mu\tilde{\alpha}_\nu^*}{2}\{\phi_k\}_\mu\{\phi_l\}_\nu^{\mathrm{T}} + \omega^2[\tilde{R}_{kl}]. \tag{7}$$

Here the matrix $[\tilde{R}_{kl}]$ accounts for the influence of higher order modes on the velocity field.

By premultiplying by $\{\phi_k\}_\mu^T[m] \times \ldots$ and postmultiplying by $\ldots \times [m]\{\phi_l\}_\nu$ the right side of equation (7) can be reduced to $\omega^2\tilde{\alpha}_\mu\tilde{\alpha}_\nu^*/2$. The modes $\{\phi_k\}_\mu$ and $\{\phi_l\}_\nu$ are normalized to the unit mass matrix (i.e., $\{\phi_k\}_\mu^T[m]\{\phi_l\}_\mu = 1$ and $\{\phi_k\}_\nu^T[m]\{\phi_l\}_\nu = 1$, while $\{\phi_k\}_\mu^T[m]\{\phi_l\}_\nu = 0$). The procedure implicitly supposes the orthogonality of the higher order modes contained in $[\tilde{R}_{kl}]$ and the lower order modes $\{\phi_k\}_\mu$, $\{\phi_l\}_\nu$ obtained by the experimental modal analysis. The described procedure rewritten in a matrix notation takes the form

$$[\tilde{\alpha}_{kl}] = (1/\omega^2)[\phi]^T[m][\tilde{V}_{kl}][m][\phi], \tag{8}$$

where $[\tilde{\alpha}_{\mu\nu}]$ represents a Hermitian matrix with the terms $\tilde{\alpha}_\mu\tilde{\alpha}_\nu^*/2$, while $[\phi] = [\{\phi_k\}_1\{\phi_k\}_2, \ldots, \{\phi_k\}_m]$ is the modal matrix containing $m$ experimentally extracted modal vectors.

When the matrix $[\tilde{\alpha}_{\mu\nu}]$ is established, the influence of higher order modes $[\tilde{R}_{kl}]$ can be evaluated by the matrix formulae

$$[\tilde{R}_{kl}] = (1/\omega^2)[\tilde{V}_{kl}] - [\phi][\tilde{\alpha}_{kl}][\phi^T]. \tag{9}$$

In fact, the $[\tilde{R}_{kl}]$ matrix represents the difference between the actual measured velocity field represented by $[\tilde{V}_{kl}]$ and the velocity field which can be expressed by using the extracted modes $[\phi] = [\{\phi_k\}_1\{\phi_k\}_2, \ldots, \{\phi_k\}_m]$ and corresponding modal factors $\tilde{\alpha}_\mu\tilde{\alpha}_\nu^*/2$. According to equation (2) and equation (9) the influence of the higher order modes can be expressed by

$$[\tilde{R}_{kl}] = \sum_\mu \frac{\tilde{\alpha}_\mu}{2}\{\phi_k\}_\mu\{\tilde{R}_l^*\}^T + \sum_\nu \frac{\tilde{\alpha}_\nu^*}{2}\{\tilde{R}_k\}\{\phi_k\}_\nu^T + \tfrac{1}{2}\{\tilde{R}_k\}\{\tilde{R}_l^*\}^T. \tag{10}$$

By postmultiplying by $\cdots \times [m]\{\phi_l\}_\nu$, the right side of equation (10) can be reduced to the vector $(\tilde{\alpha}_\nu^*/2)\{\tilde{R}_k\}$. Note that modal vectors are normalized to the unit mass matrix (i.e., $\{\phi_k\}_\nu^T[m]\{\phi_l\}_\nu = 1$ and $\{\phi_k\}_\mu^T[m]\{\phi_l\}_\nu = 0$), while the vector $\{\tilde{R}_l\}$ is a linear combination of higher order modes still considered to be orthogonal to the experimentally extracted modes (i.e., $\{\tilde{R}_l^*\}^T[m]\{\phi_l\}_\nu = 0$). The procedure can be written in matrix form as

$$[\tilde{\alpha}^*\tilde{R}] = [\tilde{R}_{kl}][m][\phi] = (1/\omega^2)[\tilde{V}_{kl}][m][\phi] - [\phi][\tilde{\alpha}_{\mu\nu}], \tag{11}$$

where $[\tilde{\alpha}^*\tilde{R}] = [(\tilde{\alpha}_2^*/2)\{\tilde{R}_l\}(\alpha_2^*/2)\{\tilde{R}_l\} \ldots (\tilde{\alpha}_m^*/2)\{\tilde{R}_l\}]$ contains $m$ vectors $\{\tilde{R}_l\}$ multiplied by half of the corresponding modal magnification factor $\tilde{\alpha}_\nu^*/2$.

The appropriate linear operator $\Lambda(\ldots)$ applied to the vectors $(\tilde{\alpha}_\nu^*/2)\{\tilde{R}_l\}$ results in the stresses due to higher order modes:

$$\Lambda((\tilde{\alpha}_\nu^*/2)\{\tilde{R}_l\}) = (\tilde{\alpha}_\nu^*/2)\{\tilde{S}_{kl}\}. \tag{12}$$

The influence of the higher order modes on the intensity field $(\tilde{\alpha}_\nu^* 2)\{\tilde{J}_k\}_\nu = (\tilde{\alpha}_\nu^*/2)\{\tilde{S}_{kl}\phi_t\}_\nu$ is then computed by using equation (6).

Once the products of modal magnification factors $\tilde{\alpha}_\mu\tilde{\alpha}_\nu^*/2$ and vectors $(\tilde{\alpha}_\nu^*/2)\{\tilde{J}_k\}_\nu$ have been evaluated from the measurements in operating conditions and the intermodal intensity vector $\{I_k\}_{\mu\nu}$ from experimental modal analysis, the computation of the corresponding structural intensity field by using equation (5) becomes a straightforward task.

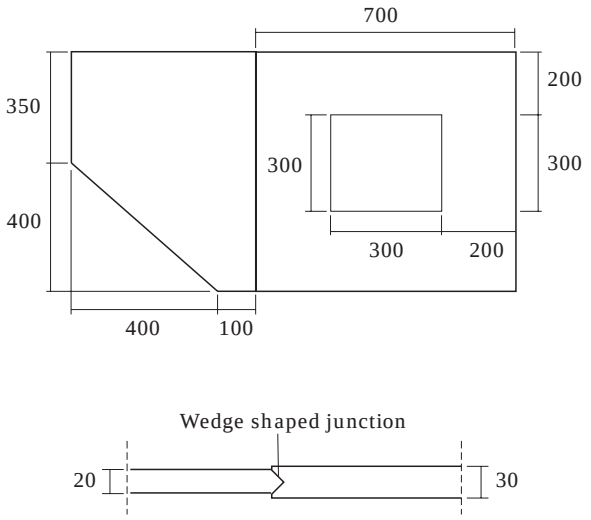


Figure 1. Plate structure used as test structure. The dimensions are specified in mm.

## 3. STRUCTURAL INTENSITY MEASUREMENTS BY THE MODAL APPROACH—APPLICATION TO AN ASSEMBLY OF TWO PLATES

### 3.1. TEST STRUCTURE

An assembly of two rigid coupled Perspex plates with different thicknesses was used as test structure. The thicker plate is rectangular with a square opening, the thinner plate is rectangular with one corner removed. These two plates are joined along a straight line groove. Figure 1 shows the test structure with main dimensions.

The measurements were performed on a uniformly distributed mesh of 339 points; see Figure 2. Three of these points, point 35, point 45, and point 294, were used as supporting points, point 172 was used as the excitation point and, finally, point 196 was used as the reference point. During the measurements the test structure was supported by three sharply pointed circular steel cones. The plate was placed horizontally on the cones. Due to the

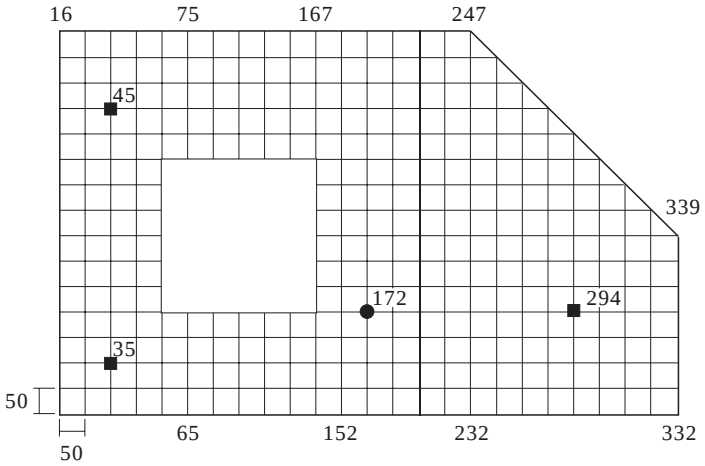


Figure 2. Mesh of observation points on the test structure. The plate is excited at point 172. The plate is supported at points 35, 45 and 294. Dimensions in mm.

weight of the plate (approximately 22·4 kg) and the small vibration amplitudes, the plate did not lose contact with supports during the measurements.

### 3.2. EXPERIMENTAL DETERMINATION OF A MODAL MODEL

A modal model of a structure is defined by the modal parameters for the modes in the model. The modal parameters of a mode are the complex resonance frequency and the mode shape vector. Experimental determination of the modal parameters requires certain input data. Normally frequency response functions of mobility type, i.e., motion over force, are used. Given a finite number of observation points, the mobilities can be written as a quadratic matrix. Under certain conditions, see reference [14] for an example, all modes with resonance frequencies within the analyzed frequency band can be identified from one column (or one row) of the mobility matrix. In the case considered here the structure is excited at one single point during operation. Thus, the column corresponding to this point contains all modal information needed to calculate the vibrational response.

The measurements were performed by using the experimental set-up shown in Figure 3. The test structure was excited with white noise at the excitation point 172 by using a shaker. An internal source in the FFT analyzer was used as a source signal. The excitation force was measured using a piezoelectric force transducer mounted directly at the excitation point 172. The response acceleration was measured by using a piezoelectric accelerometer. The force and the acceleration signals were both conditioned in charge amplifiers. Finally an FFT analyzer was used to estimate the mobility between the excitation point and the response point.

The measurements were performed in the frequency range from 0–1 kHz with the frequency resolution 1·25 Hz. Each mobility was estimated by using frequency domain averaging to reduce influence from random errors. A typical mobility measured on the test structure is shown in Figure 4.

When all mobilities with reference to point 172 had been measured, a commercial modal analysis software (SMS Star Modal) was used to extract modal parameters of the test structure. The final results were obtained by using two parameter extraction routines denoted *Global Frequency and Damping* and *Global Residues*. Ranging from 19–550 Hz, 20 modes of the test structure were identified; see Table 1. The method validated in this paper relies on the orthogonality of modes. Hence, the scalar product between all mode

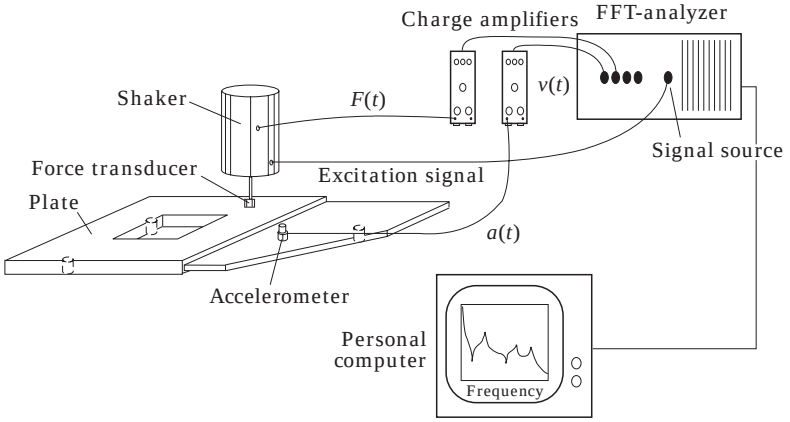


Figure 3. Experimental set-up during mobility measurements.

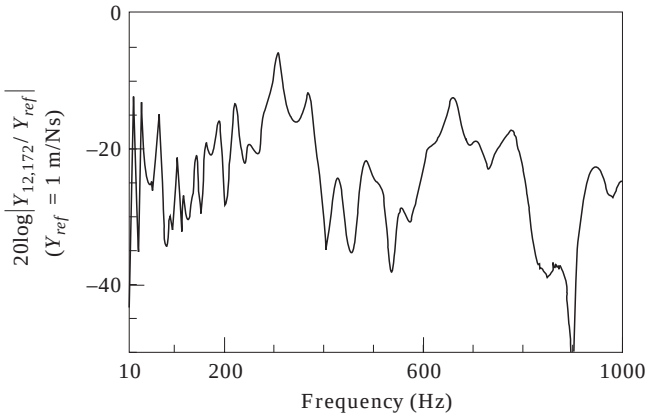


Figure 4. A typical accelerance function (magnitude) for the plate.

shape vectors was calculated and normalized. Two of these products are approximately 0·02, the rest are less than or equal to 0·01. Thus, the identified modes can be considered to be orthogonal. It should be noted that the boundary conditions realized for the real structure only approximated the simply supported conditions assumed in the calculations. The motion at the supporting points was measured by placing accelerometers at point 35, at point 45 and at point 294 on the upper surface of the plate. The motion at these points was found to be small but non-zero. Hence the assumed simply supported boundary conditions were reasonably closely realized during the measurements.

The modal displacements are evaluated at the nodes of the structure mesh shown in

TABLE 1

*Modal frequencies and loss factors*

| Mode | Resonance frequency (Hz) | Loss factor |
|---|---|---|
| 1 | 19·1 | 0·12 |
| 2 | 33·5 | 0·052 |
| 3 | 70·4 | 0·070 |
| 4 | 90·4 | 0·060 |
| 5 | 99·4 | 0·066 |
| 6 | 106 | 0·055 |
| 7 | 143 | 0·041 |
| 8 | 161 | 0·048 |
| 9 | 191 | 0·048 |
| 10 | 221 | 0·044 |
| 11 | 246 | 0·048 |
| 12 | 275 | 0·042 |
| 13 | 294 | 0·049 |
| 14 | 306 | 0·043 |
| 15 | 371 | 0·047 |
| 16 | 389 | 0·034 |
| 17 | 429 | 0·042 |
| 18 | 481 | 0·043 |
| 19 | 523 | 0·045 |
| 20 | 550 | 0·045 |

Figure 2. The values inside the rectangular or triangular cells of the structural mesh are computed by averaging the corresponding nodal values.

$$w_c = \frac{1}{n}\sum_n w_n. \tag{13}$$

It should be noted that the modal displacements at the nodes of the structural mesh are identified by the index $n$ while the corresponding values at the centres of the cells of the mesh have an index $C$. The same convention is used for the rotations, for the internal forces and for the internal moments due to modal displacements. These are computed by using the derivatives of the displacement field, the material properties and the geometry of structure. The required derivatives of the displacement field are estimated by using a finite difference technique. The rotations of the plate can be estimated by using the first derivatives of the lateral displacements:

$$\vartheta_{xC} \approx \partial w/\partial y|_C \approx \Delta w_n/\Delta y, \qquad \vartheta_{yC} \approx \partial w/\partial x|_C \approx -\Delta w_n/\Delta x. \tag{14}$$

Here the finite difference type operators $\Delta(...)/\Delta x$ and $\Delta(...)/\Delta y$ are defined as follows: for a triangular finite difference cell,

$$\Delta w_n/\Delta x = [2w_J - (w_K + w_I]/2a, \qquad \Delta w_n/\Delta y = [2w_K - (w_J + w_I]/2b, \tag{15}$$

and for a rectangular finite difference cell (see Figure 5).

$$\Delta w_n/\Delta x = [(w_K + w_J) - (w_L + w_I)]/2a,$$
$$\Delta w_n/\Delta y = [(w_K + w_L) - (w_J + w_I)]/2b. \tag{16}$$

The estimates of the plate rotations $\vartheta_{xC}$ and $\vartheta_{yC}$ are computed at each finite difference cell of the mesh defined in Figure 2. The rotations at the nodes $\vartheta_{xn}$ and $\vartheta_{yn}$ are then evaluated by interpolating and/or extrapolating at the central values $\vartheta_{xC}$ and $\vartheta_{yC}$. For such purposes an averaging procedure using the values at the centres of the cells with a common node is used. Such a procedure is sensible only for smooth functions. For example the curvatures (defined by the second derivatives of the displacement field) of the test structure cannot be treated in the same way. The averaging procedure applied to the plate curvatures would completely mask the jumps of the second derivatives at the interface of the plates with different thickness. On the contrary the internal forces and moments are the smooth functions in the whole domain of the plate structure and the averaging procedure is allowed. The internal moments $M_{xC}$, $M_{yC}$, $M_{xyC}$ at the centres of finite difference cells are evaluated by using the derivatives of the rotations and material properties of the plate:

$$M_{xC} \approx [Eh^3/12(1 - \nu^2)](\Delta\vartheta_{yn}/\Delta x + \nu\,\Delta\vartheta_{xn}/\Delta y), \tag{17}$$

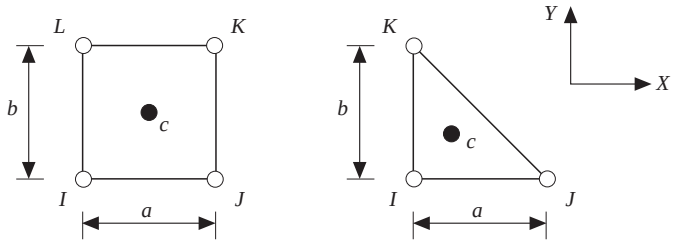


Figure 5. Quadrilateral and triangular cells used for the finite difference computation.

$$M_{yC} \approx [Eh^3/12(1-v^2)](\Delta\vartheta_{xn}/\Delta y - v\,\Delta\vartheta_{yn}/\Delta x), \tag{18}$$

$$M_{xyC} \approx [Eh^3/6(1+v)]\tfrac{1}{2}(-\Delta\vartheta_{xn}/\Delta y + \Delta\vartheta_{yn}/\Delta x). \tag{19}$$

Here $E$ is the Young's modulus, $v$ is the Poisson's ratio and $h$ is the plate thickness. It should be noted that the method used imposes that the material properties and the thickness of the plate be constant within each finite difference cell, but different properties can be used for different element cells. Once the internal moments are calculated at the centres of the cells, the corresponding nodal values $M_{xn}$, $M_{yn}$, $M_{xyn}$ are computed by using the interpolation/extrapolation procedure described previously. The computation procedure for the shear forces $Q_{xC}$, $Q_{yC}$ involves the moments evaluated at the nodes corresponding to the finite difference cell:

$$Q_{xC} \approx \Delta M_{xn}/\Delta x + \Delta M_{xyn}/\Delta y, \qquad Q_{yC} \approx \Delta M_{yn}/\Delta y + \Delta M_{xyn}/\Delta x. \tag{20, 21}$$

The displacements, rotations, internal moments and internal forces computed in the cell centres are used to evaluate the structural intensity. The computation procedure developed in the present paragraph defines a linear operator $\Lambda(...)$ used in equation (4). The members column vectors $\{I_k\}_{\mu v}$, defined by equation (6), are constituted by using two components of the intensity which correspond to directions $x$, $y$ of the global co-ordinate system:

$$I_{x\mu v} = Q_{x\mu} w_v + M_{x\mu}\vartheta_{yv} - M_{xy\mu}\vartheta_{xv}, \qquad I_{y\mu v} = Q_{y\mu} w_v - M_{y\mu}\vartheta_{xv} + M_{xy\mu}\vartheta_{yv}. \tag{22, 23}$$

The displacements $w_v$ and rotations $\vartheta_{xv}$, $\vartheta_{yv}$ correspond to the mode denoted with a Greek letter $v$, while the internal moments $M_{x\mu}$, $M_{y\mu}$, $M_{xy\mu}$ and internal forces $Q_{x\mu}$, $Q_{y\mu}$ correspond to the mode denoted with a Greek letter $\mu$. Positive values of these quantities are defined in Figure 6.

### 3.3. VIBRATIONAL MEASUREMENTS IN OPERATING CONDITIONS AND EVALUATION OF STRUCTURAL INTENSITY FIELD

To evaluate the structural intensity using the experimentally determined modal parameters, some vibrational measurements in operating conditions were required, too. Operating conditions were defined as the stationary conditions obtained when the plate structure was excited with a random force perpendicular to the plate at point 172. The point 196 is reference point.

The following measurements were performed during operation: the power spectral density of the excitation force $\tilde{F}$, $G_{FF}(\omega) = \tilde{F}\tilde{F}^*/2$; the power spectral density of the

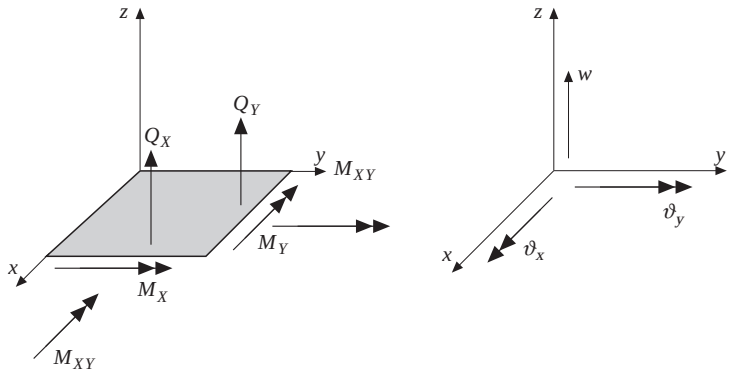


Figure 6. Plate element; its co-ordinate system with positively defined internal forces and displacements.

acceleration at the reference point $\tilde{a}_R$, $G_{RP}(\omega) = \tilde{a}_R\tilde{a}_R^*/2$; the frequency response function between the acceleration at the reference point $\tilde{a}_R$ and the excitation force $\tilde{F}$; $\tilde{H}_{RF}(\omega) = \tilde{a}_R/(\tilde{F})$; the frequency response functions between the accelerations at each mesh point $\tilde{a}_i$ and the reference point $\tilde{a}_R$, $\tilde{H}_{iR}(\omega) = \tilde{a}_i/\tilde{a}_R$. All these measurements were performed in the range from 125–225 Hz with a frequency resolution of 0·25 Hz. The experimental set-up was basically the same as the one used during the modal analysis measurements. All required specta were calculated by a FFT analyzer. Frequency domain averaging was used to reduce influence of random errors. Once the transfer functions are established, the spectra defining the vibrations in operating conditions are computed:

$$\tilde{v}_i\tilde{v}_j^*/2 = (1/\omega^2)G_{RR}(\omega)\tilde{H}_{iR}(\omega)\tilde{H}_{jR}^*(\omega). \tag{24}$$

The spectral matrix $[\tilde{V}_{kl}]$, which completely defines the vibrations in operating conditions, is established by using the computed spectral data $\tilde{v}_i\tilde{v}_j^*/2$; see equation (24).

### 3.4. RESULTS AND DISCUSSION

The modal parameters, and vibrations in operating conditions, are used to compute the structural intensity distribution within the plate structure; see Figure 1. The mass matrix of the structure considered needed for the computation is determined by using a finite element technique and the mest shown in Figure 2.

In Figure 7 the frequency spectra of vibrational velocities for the operating condition are presented. The spatial average of squared RMS velocity of the plate is indicated by the thin line, while the thick line is used to present the squared RMS velocity of the reference point. The spatial distribution of vibrations within the test structure is shown in Figure 8. The squared RMS velocities measured at the nodes of the mesh are interpolated within the finite difference cells and presented in the grey colour scale. The darkest areas indicate the maxima of the vibrational velocities.

The position of the shaker is indicated by the letter S. The position of the shaker cannot be deduced from the RMS velocity map. The maxima of the velocity field are not in the excitation area.

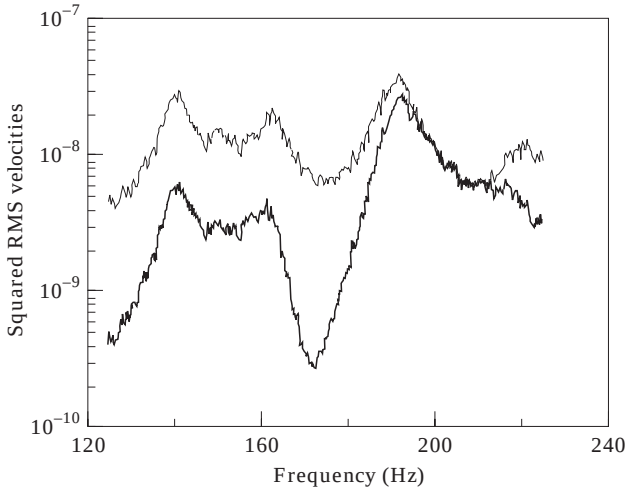


Figure 7. Squared RMS velocities in the plate structure as a function of the frequency. Thin line, spatial average of squared RMS velocity of the plate; thick line, squared RMS velocity of the reference point.

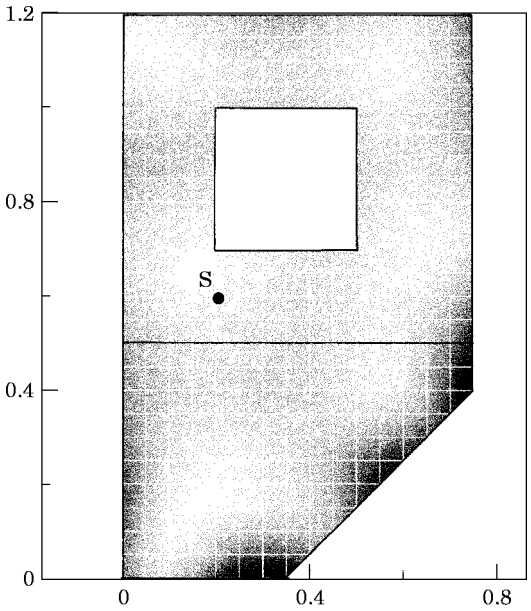


Figure 8. Spatial distribution of RMS velocities within the plate-like structure. Darkest areas indicate the maxima of the velocity field. The excitation point is indicated by the letter S.

On the contrary, the structural intensity field shown in Figure 9 might be of help in the location of the source of structural vibrations. The structural intensity vectors show the net energy flow coming out from the point of the shaker application. The magnitudes of

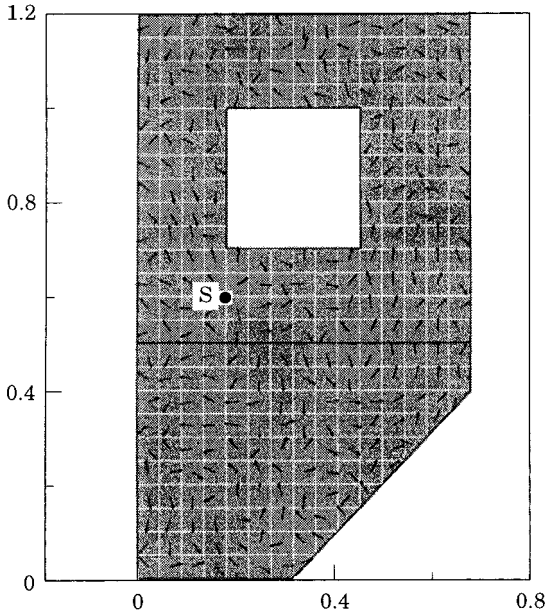


Figure 9. Structural intensity distribution within the plate-like structure; the excitation point is indicated by the letter S.

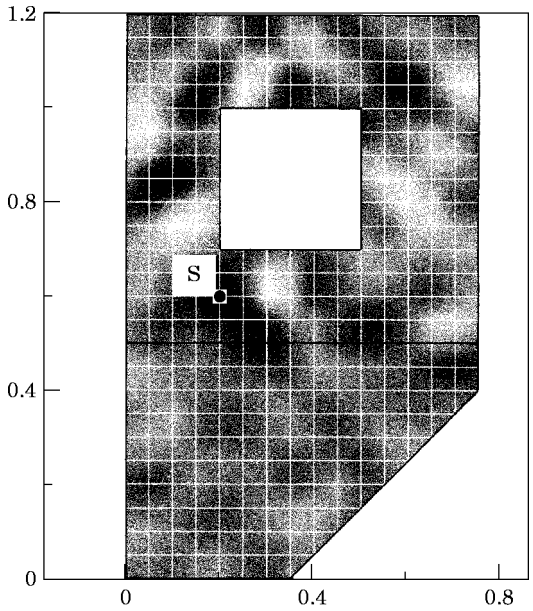


Figure 10. Divergence of structural intensity. Darkest areas indicate the maxima of the divergence of structural intensity (i.e. power input areas). The excitation point is indicated by the letter S.

the vectors are given in the logarithmic scale in Figure 9. The divergence of structural intensity vectors is shown in Figure 10. The darkest area indicates the maxima of the divergence and the areas of the input of vibrational energy: i.e., the possible source locations. The actual shaker position denoted with S coincides with the maximum of the divergence of structural intensity; see Figure 10.

The power $P_F(\omega)$, injected by the shaker to the structure, can be computed by using the velocity $\tilde{v}_F$ and the force $\tilde{F}$ measured at the excitation point:

$$P_F(\omega) = \tilde{F}\tilde{v}_F^*/2. \tag{25}$$

The power injected by the shaker is then dissipated in the structure. The spatial distribution of the energy propagated within the structure is defined with the structural intensity field, which in the case of plate type structures represents the energy propagating through the unit length. According to the principle of conservation of energy, the power injected to the plate can be deduced by integrating the component of the structural intensity vector, which is normal to a closed curve (L) enclosing the vibrational source:

$$P^I(\omega) = \oint_L \vec{I} \cdot \vec{n}\, \mathrm{d}l. \tag{26}$$

Since the energy is dissipated while propagating through the damped structure the curve should be as close to the source as possible. In this way the difference between the real input power and the input power evaluted by the integration of the structural intensity is reduced. In the present analysis the chosen curve is a rectangle in which the corners of the four finite difference cells have a common node at the excitation point S. The integral defined by equation (26) is estimated by using an appropriate numerical procedure and the defined integration curve. In the frequency range considered (125–225 Hz), there is a close agreement between the results obtained by the two methods.

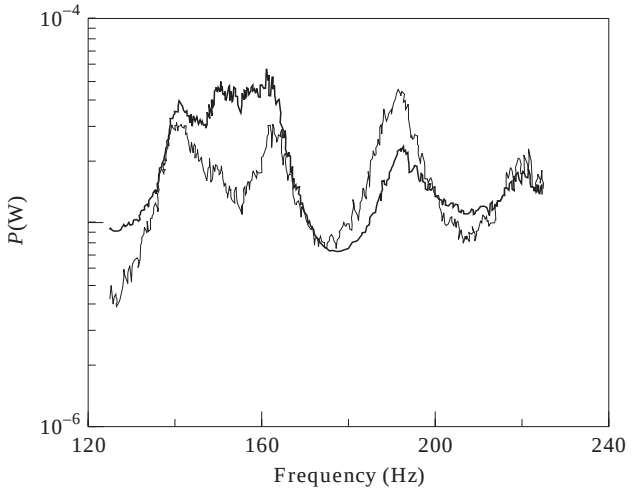


Fig. 11. Power injected into the plate-like structure as a function of the excitation frequency. Thin line, directly measured injected power; thick line, indirectly injected evaluated by using the structural intensity distribution.

The total input power measured directly equals 2·0 mW, while the same power estimated by the integration of structural intensity field is 1·7 mW. The frequency distribution of the power injected to the test structure is presented in Figure 11. The thin line indicates the injected power obtained by the direct measurements of force excreted by the shaker and of the velocity of the excitation point according to equation (25). The thick (dark) line indicates the input power estimated by the integration of struuctural intensity according to equation (26).

## 4. CONCLUDING REMARKS

An experimental method for evaluation of structural intensity field by using a normal mode approach and the vibrations in the operating condition has been developed. The method has been applied to a structure which consists of two joined Perspex plates. The structural intensity field and its divergence has been evaluated within the structure. The maximum of the divergence of structural intensity, evaluated by using the method developed, indicated clearly the position of the shaker which was used as the source of vibrational energy in the experimental set-up. The power injected into the structure was then estimated by integrating the structural intensity vectors over a closed curve enclosing the excitation point. The results obtained have been compared with the results of direct measurements of the input power performed by an impedance head. There is a close agreement between the results obtained by the two methods.

The method presented for structural intensity evaluation, based on the modal approach, is well suited for assembled thin-walled structures. At persent only assemblies of plates have been treated but the method can be easily extended to plate–beam assemblies.

## ACKNOWLEDGMENT

The research work was supported by The European Union under the BRITE-EURAM programme as the part of the contract BRE2-CT 92-0332 of project 5975-SILENTA.

## REFERENCES


1. D. U. Noiseux 1970 *Journal of Acoustical Society of America* **47**, 238–247. Measurement of power flow in uniform beams and plates.
2. G. Pavic 1976 *Journal of Sound and Vibration* **49**, 221–230. Measurement of structure borne wave intensity, part I: formulation of the methods.
3. J. W. Verheij 1976 *Journal of Sound and Vibration* **70**, 133–138. Cross-spectral density methods for measuring structure borne power flow on beams and pipes.
4. P. Rasmussen and G. Rasmussen 1983 *Proceedings of the* 11*th International Congress on Acoustics*, *Paris* **6**, 231–234. Intensity measurements in structures.
5. X. Carniel and J. C. Pascal 1985 *Proceedings of the Second International Congress on Acoustic Intensity*, 23–26 *September*, *Senlis*, 211–217. Charactéristiques de propagation et measures du flux d'énergie vibratoire dans les barres (Characteristics and measurements of the energy flow in beams) (in French).
6. J. C. Pascal, T. Loyau and J. A. Mann III 1990 *Proceedings of the Third International Congress on Intensity Techniques*, 27–29 *August*, *Senlis*, 197–204, Structural intensity from spatial Fourier transformation and BAHIM acoustical holography method.
7. R. C. Fuller 1981 *Journal of Sound and Vibration* **75**, 207–228, The effect of wall discontinuities on the propagation of flexural waves in cylindrical shells.
8. A. J. Romano, P. B. Abraham and E. G. Williams 1990 *Journal of the Acoustical Society of America* **87**, 1166–1175, A Poynting vector formulation for thin shells and plates, and its application to structural intensity analysis and source localisation, part I: theory.
9. G. Pavic 1992 *Journal of Sound and Vibration* **154**, 411–429. Vibroacoustical energy flow through straight pipes.
10. G. Pavic 1990 *Proceedings of the Third International Congress of Intensity Techniques*, 27–29 *August*, *Senlis*, 21–28. Energy flow induced by the structural vibrations of elastic bodies.
11. L. Gavric and G. Pavic 1990 *Proceedings of the Third International Congress on Intensity Techniques*, 27–29 *August*, *Senlis*, 207–214. Computation of structural intensity in beam-plate structures by numerical modal analysis using FEM.
12. L. Gavric 1992 *Proceedings of the* 17*th International Seminar on Modal Analysis*, 21–25 *September*, *Leuven*, 193–205. Computation of structural intensity for a wide band excitation using normal mode approach.
13. L. Gavric and G. Pavic 1993 *Journal of Sound and Vibration* **164**, 29–43. A finite element method for computation of structural intensity by normal mode approach.
14. D. J. Ewins 1984 *Modal Testing*: *Theory and Practice*. Letchworth, Herefordshire, UK: Research Studies Press.